Longan: Ultra-Low-Power, Long-Range LoRa Receiver for LPWANs

Mingzhe Li
Department of Computer Science
City University of Hong Kong
Hong Kong, Hong Kong
mingzheli8-c@my.cityu.edu.hk

Tao Chen
Independent Researcher
Plano, Texas, USA
tachen.cs@gmail.com

Zhenjiang Li
Department of Computer Science
City University of Hong Kong
Hong Kong, Hong Kong
zhenjiang.li@cityu.edu.hk

Abstract

Low-Power Wide-Area Networks (LPWANs) are essential for IoT connectivity, but they face a longstanding fundamental challenge: achieving both continuous receiver availability and long-term battery operation without compromising network performance. In low-duty-cycle modes like LoRaWAN's Class A or B, data timeliness and network throughput are limited, and devices are deaf to peer transmissions, restricting topologies to a single hop, hindering scalability in practical applications. While Class C enables always-on operation for real-time communication and multi-hop networking, commercial LoRa transceivers consume up to 42.4 mW in this mode, rendering sustained battery-powered deployments infeasible. Recent low-power designs cut consumption to sub-milliwatt levels but limit communication ranges to mere hundreds of meters, undermining LPWAN's "wide-area" vision. This paper introduces Longan, the first LoRa receiver to overcome this power-range tradeoff boundary, enabling kilometer-scale links with a power of about 1 mW only. Longan achieves this via two breakthroughs: (1) We design a novel LoRa receiver analog radio frequency (RF) front-end that exploits negative differential resistors for high-efficiency signal amplification while simultaneously reducing power consumption by 2–3 orders of magnitude; (2) Building on this, we further introduce an architectural decoupling of detection and demodulation, and design a lightweight analog dechirping circuit using our front-end. This circuit enables always-on preamble detection at just one-tenth the power of digital counterparts, triggering COTS demodulation only on demand. Evaluation shows that Longan sustains continuous detection at 1.16 mW, a 36× reduction from COTS LoRa, while preserving sensitivity within 3–13 dB of commercial devices and enabling long-range communication.

CCS Concepts

• **Hardware → Wireless devices**; • **Networks → Wireless access points, base stations and infrastructure**.

Keywords

LPWAN, Ultra-low-power Communication, LoRa, IoT

SenSys '26, Saint Malo, France

ACM ISBN 979-8-4007-2309-4/26/05
https://doi.org/10.1145/3774906.3802753

ACM Reference Format:
Mingzhe Li, Tao Chen, and Zhenjiang Li. 2026. Longan: Ultra-Low-Power, Long-Range LoRa Receiver for LPWANs. In *ACM/IEEE International Conference on Embedded Artificial Intelligence and Sensing Systems (SenSys '26), May 11–14, 2026, Saint Malo, France.* ACM, New York, NY, USA, 14 pages. https://doi.org/10.1145/3774906.3802753

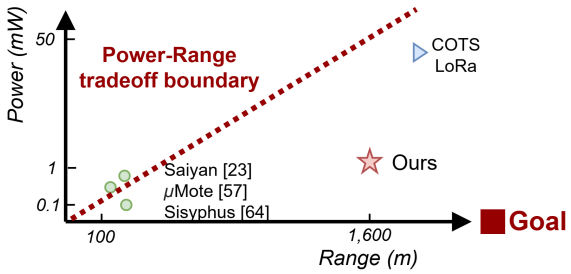

Figure 1: Longan overcomes the power-range tradeoff boundary in LoRa receiver design, enabling ultra-low power operation without compromising long-range communication.

1 Introduction

LPWANs [4, 45] have become as a cornerstone technology for the Internet of Things (IoT) and smart cities [7, 29, 32, 65, 68, 71], enabling connectivity across vast areas while maintaining minimal energy consumption. Among these technologies, LoRaWAN [26, 66, 69] has emerged as the *de facto* standard for large-scale deployments because it can provide kilometer-scale communication ranges and allows for years of battery-powered operation [22, 55].

However, commercial off-the-shelf (COTS) LoRa receivers achieve long-term battery life only in *low-duty-cycle* modes like Class A (sleeping) or Class B, where receiver activity is limited to less than 1% of operational time [53]. This paradigm severely limits *data timeliness*, *network throughput*, and restricts connectivity to a *single hop*, limiting the scalability in practical applications like industrial monitoring [25] and in-the-wild environmental sensing [12]. In contrast, Class C enables *always-on operation* for real-time communication and multi-hop coordination [53], but at a prohibitive energy cost. For example, transceivers like the widely used SX1278 consume up to 42.4 mW in Class C mode, and can only operate continuously for 6.3 days using common 2 AA batteries (2000 mAh), making long-term deployment impractical.

To bridge this gap, prior efforts have revisited the superheterodyne architecture of LoRa receivers (§2) and proposed low-power alternatives that reduce consumption during continuous operation by eliminating power-hungry components. For example, Saiyan [23] uses a Surface Acoustic Wave (SAW) filter to bypass down-conversion

and Analog-to-Digital Converters (ADCs), while μMote [57] and Sisyphus [64] explore Low-Noise Amplifier (LNA)-free designs with passive components and LC resonance. However, these state-of-the-art (SOTA) designs expose a critical limitation. The rationale of these designs is to eliminate energy-consuming RF amplifiers (*e.g.*, LNAs) from receiver, but this drastically reduces receiver sensitivity, limiting communication range to mere hundreds of meters. Sisyphus, for instance, achieves about 107 meters, and μMote extends to 400 meters under high transmitting power(1 W) — far short of the kilometer-scale ranges of COTS LoRa devices with LNA amplifier, a necessary defining feature of LoRaWAN [4, 55] and a key reason for its wide adoption in real-world applications [45].

These limitations highlight a fundamental **power–range tradeoff boundary**, as illustrated in Figure 1 — lowering power compromises range, while increasing range boosts power. This tradeoff motivates our central question: *Can we overcome this boundary to deliver both ultra-low power and long-range, high-availability LoRa communication?* In this paper, we propose Longan, the first LoRa receiver design that overcomes the power–range tradeoff boundary, achieving both low power consumption and long-range communication. This allows LoRa nodes to be woken up frequently, thereby improving availability while still enabling long-term deployment. Longan's breakthroughs stem from two key designs.

(1) Ultra low-power RF front-end. In receiver hardware, amplifier is a major energy consumer [42, 57]. Traditional amplifiers rely on Bipolar Junction Transistors (BJTs), which convert less than 0.01% of the supplied energy to useful RF amplification merely [41, 42]. Despite their low conversion efficiency, eliminating them would greatly reduce receiver's sensitivity, weakening the communication range as observed in recent designs.

Longan takes a different approach. Instead of removing the amplifier, we design a novel, ultra low-power amplifier using tunnel diodes (TDs) [62]. TDs possess unique characteristics, with their current-voltage (I-V) curves containing a *negative* slope. When a TD amplifier operates within this range, it generates a **negative differential resistance** [30], *i.e.*, when we increase the voltage, the current decreases. This characteristic can be exhibited under extremely low voltage power supply and can be used to amplify signals. Thus, we can reduce power consumption while amplifying signal, making it three orders of magnitude lower than BJT-based amplifiers while maintaining comparable amplification performance.

(2) Detection-triggered demodulation. Another major source of power consumption in the receiver is the digital baseband, as shown in Figure 2. It involves digital domain operations such as FFT and dechirping for decoding packets, which can rapidly consume power if nodes remain awake for extended periods to achieve high availability, even with an low-power analog RF front-end.

Inspired by wake-up receivers [38, 59], we propose to **decouple** LoRa receiver's processing into **packet detection** (continuous channel monitoring) and **on-demand demodulation** (triggered only when a packet is detected). Since detection does not require decoding precise symbols, a lightweight analog dechirping circuit can be designed in the digital intermediate frequency (IF) step without using the digital baseband when no packet is detected. Compared to existing receivers that require digital baseband demodulation results to determine packet presence each time, we design and connect a lightweight analog detector after the RF front-end for detection,

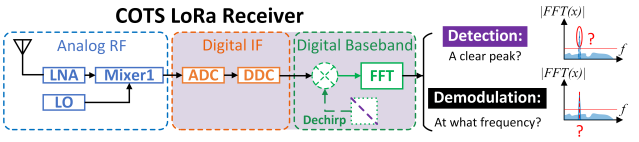

Figure 2: The architecture of a legacy COTS LoRa receiver includes three key components. Unless demodulated, it is unknown whether there are any LoRa symbols.

significantly reducing power consumption. This allows for frequent detection operations, enabling nodes to operate at high duty cycles without impacting long-term deployment. Furthermore, decoding performance and communication range are guaranteed because demodulation is still performed using a commercial demodulator.

In summary, the core idea of Longan is to design a low-power RF front-end, and to effectively decouples the receiver's responsibilities into low-power packet detection and on-demand demodulation (only triggered after detection). This allows packet detection to be performed frequently (even continuously) while maintaining low receiver power consumption, ensuring node availability and long-term deployment without sacrificing communication range. While above designs form the foundation of Longan, we further solve technical challenges in realizing it: 1) addressing the instability of TD amplifiers and the failure of conventional RF mixers; 2) solving the phase misalignment between the local oscillator (LO) and incoming preambles in packet detection. We propose a hardware-software co-designed solution to address these challenges.

We develop Longan prototype and perform extensive experiments to evaluate its performance, from basic circuit characteristics to full network applications. We compare it against COTS LoRa devices and SOTA low-power receivers (Sisyphus [64], μmote [57]) as baselines. Extensive experiments demonstrate that Longan achieves continuous preamble detection at 1.16 mW, which is 36× lower than COTS LoRa, while retaining sensitivity within 3–13 dB of commercial devices and supporting long-range communication.[1]

The contributions of Longan are summarized as follows:

- We present the first LoRa receiver design (to our best knowledge) that overcomes the power–range tradeoff boundary, enabling low-power, high-availability, long-range LoRa communication.
- We introduce novel techniques featuring TD-based amplification/oscillation and decoupled analog detection, systematically addressing the identified challenges.
- We prototype Longan and conduct extensively evaluations from basic circuit characteristics to full network applications. Results demonstrate promising performance and significant improvement gains compared to the SOTA approaches.

Longan allows LoRa receivers to enjoy Class C mode functionality while consuming similar energy previously consumed by the receivers operating in Class A or B mode (LoRa nodes can be configured to operate in Class A, B, or C modes). It also unlocks network advancements like energy-efficient CSMA protocols and scalable, low-latency multi-hop networking for battery-powered LoRa.

[1] Due to site distance limitations, we use a transmit power of only 4–7 dBm at a LOS distance of 700 m for testing and further derive the equivalent distance over 1600 m using the official LoRa range calculator [56] at a standard 20 dBm transmit power.

Table 1: Receiver's signal gain (green) and power (orange) breakdown comparison based on our measure and literature.

	Analog RF	Digital IF	Baseband
COTS [51, 54]	>20 dB gain	digital gain	
	25 mW–42 mW		
Sisyphus [64]	0 dB gain	6 dB gain	\
	0 μW	**286 μW**	**163 μW**
Longan	42 dB gain	24 dB gain	\
	496 μW	**657 μW**	**6 μW**

2 Preliminary

2.1 Background: COTS LoRa Receiver

COTS LoRa receiver adopts a *superheterodyne* architecture for signal reception. As illustrated in Figure 2, the signal processing chain includes three main stages: 1) Analog RF front-end, 2) Digital IF, and 3) Digital Baseband.

- **Analog RF front-end**: The incoming LoRa signal from antenna is first amplified by an RF amplifier (*e.g.*, LNA). The amplified signal is then down-converted by a mixer and stabilized with a high-frequency carrier signal generated by local oscillator (LO), *i.e.*, phase-locked loop (PLL). The signal then proceeds to the next module.
- **Digital IF**: In this module, the signal is digitized by a high-power ADC and further processed by a digital down-converter (DDC) to generate a digital baseband signal.
- **Digital Baseband**: This module performs demodulation operations. Specifically, the digital baseband signal is dechirped by multiplying it with a down-chirped signal, and then fast Fourier transform (FFT)-based peak detection is applied to identify signal-tone outputs for demodulating each symbol. If a clear peak is detected, the frequency point corresponding to the peak is the bits carried by this LoRa symbol.

When a legacy receiver is on, it can only know the arrival of LoRa symbols after FFT. In other words, the entire pipeline in Figure 2 is *multiplexed* for simultaneous packet *detection* and *demodulation*, which is the main reason limiting the battery life of legacy LoRa receivers at high duty cycles for high availability.

2.2 Power–Range Tradeoff

Table 1 summarizes the power-range tradeoff in different types of LoRa receiver designs.

1) COTS. The design rationale of legacy receivers is to obtain sufficient signal gain for reliable packet reception. As shown in Table 1, legacy LoRa receivers typically provide more than 20 dB sensitivity gain, primarily from the amplifier in the RF front-end. Subsequent digital IF and baseband modules further process the signal through ADC, digital conversion, and dechirping to extract additional digital gain. However, these operations come at the cost of higher power consumption (25–42 mW) in total.

2) SOTA. To avoid high power consumption, SOTA designs, such as Sisyphus [64], employ the opposite strategy, completely eliminating amplifiers and replacing digital IF/baseband with envelope detectors and comparators. While this greatly reduces power consumption (from tens of mW to tens or hundreds of μW), it sacrifices approximately 20 dB of RF front-end sensitivity, resulting in a significantly reduced communication range, *e.g.*, to about 107 meters [64]. One might ask whether it is possible to improve sensitivity while maintaining acceptable power consumption by adding amplifiers, thus achieving a balance. To verify this, we integrate two RF amplifiers in both Sisyphus and μmote and find that when their communication range is extended (*e.g.*, 1.6 km), the power consumption is comparable to COTS receiver (25–34 mW in §6).

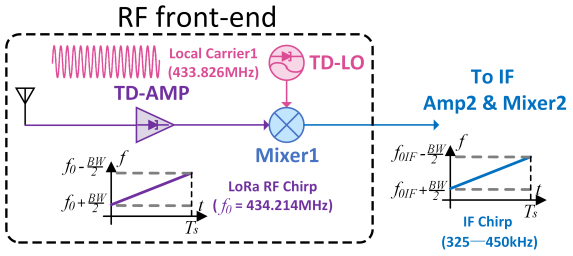

Figure 3: Illustration of the RF front-end in Longan.

3) Ours. To break this power-range tradeoff boundary, we take a different approach in Longan by designing a novel amplifier that can amplify the signal while remaining low power simultaneously. As shown in Table 1, our amplifier achieves 42 dB gain at the power consumption of 496 μW only. Furthermore, the IF design further brings 24 dB gain to ensure the communication range. With 6 μW additional power consumption from the baseband detector, Longan can perform the packet symbol detection. As thoroughly measured in our evaluation, the overall power consumption of Longan is 1.16 mW even when it continuously detects incoming packet (preamble) symbols, which is 36x lower than the COTS receivers.

2.3 Benefits and Design Overview

Long-range, low-power receivers make it practical for LoRa nodes to wake up frequently (or even stay on all the time) for packet detection, which can bring the following benefits to LoRaWANs:

- **Network management**: It enables LoRa nodes to receive notifications and data from the gateway in time, and to perform CSMA to avoid collision with other ongoing packets.
- **Network traffic**: It can improve sensing data freshness, timeliness and network throughput.
- **Network topology**: It enables relay nodes to hear data from other nodes for forwarding, thereby achieving multi-hop networking and allowing LoRaWAN to cover a wider area.

To harvest above benefits, Longan introduces two main designs:

- **Low-power front-end (§3)**: It designs a TD-based amplifier, a dedicated local oscillator and down-conversion mixer.
- **Packet detector (§4)**: It decouples detection and demodulation and introduces an efficient LoRa preamble detector.

We elaborate on these two designs in the following two sections.

3 RF Front-end of Longan

As shown in Figure 3, we first present our Low-Noise TD-based Amplifier (TD-AMP), which provides effective RF signal amplification while maintaining ultra-low power consumption (§3.1). We then introduce our customized local oscillator (TD-LO) (§3.2) and RF mixer (Mixer1) (§3.3) to down-convert signal to IF band while addressing the signal loss and RF/IF leakage issue due to TD components.

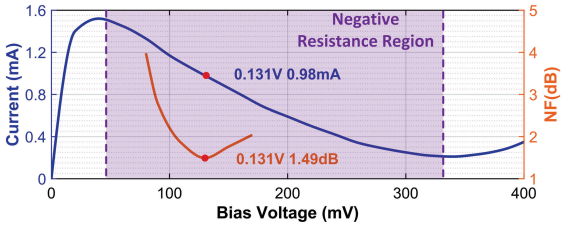

Figure 4: I-V curve and noise figure (NF) of a TD 1I104A. We apply the bias voltage at 0.131 V for amplification, achieving the best $NF = 1.49$ dB. The required current for amplification is 0.98 mA, 1–2 orders of magnitude lower than that of a typical BJT.

3.1 TD-based Low-Noise Amplifier (TD-AMP)

This design component strives to provide RF signal amplification with ultra-low power. In existing RF receiver systems, amplifiers play a critical role in enabling detection within low noise figure (NF) by amplifying weak input signal [19, 46]. However, traditional RF amplifiers typically rely on bipolar junction transistors (BJTs) for signal amplification, which demand hundreds of mA to achieve around 20 dB gain [57]. Inside it, the base current I_B consists of both the signal current I_{signal} and the bias current I_{bias} ($I_B = I_{signal} + I_{bias}$). To maintain operation in the linear active region across RF frequencies, a constant I_{bias}, typically on the order of hundreds of μA to mA, is required, even in the absence of an input signal. This results in persistently high static power consumption and extremely low energy efficiency (*e.g.*, $\ll 0.01\%$) [41, 42], severely limiting the applicability of BJT-based AMPs in low-power IoT scenarios.

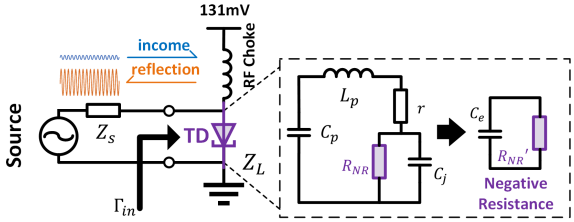

Figure 5: Working principle of TD-based amplification.

We employ a tunnel diode (TD) as the key enabler for achieving high RF amplification at μW-level power consumption [2, 61–63]. TDs exhibit negative resistance characteristics arising from quantum tunneling effects [62]. As shown in Figure 4, when bias voltage is excited at its *negative-resistance region*, the diode's **current decreases with increasing voltage**, producing a distinctive negative differential slope in the I–V curve.

(1) Why negative resistance can amplify signal? As shown in Figure 5, once the incoming signal travels (from left to right) into the TD, the signal will both get reflected and amplified. The reflection coefficient Γ_{in} can be defined as the amplitude ratio between the reflected signal and incoming signal, which can be calculated by:

$$\Gamma_{in} = \frac{Z_L - Z_S^*}{Z_L + Z_S} = \frac{\mathbf{R}\{Z_L\} + j\mathbf{I}\{Z_L\} - (\mathbf{R}\{Z_S\} - j\mathbf{I}\{Z_S\})}{\mathbf{R}\{Z_L\} + j\mathbf{I}\{Z_L\} + (\mathbf{R}\{Z_S\} + j\mathbf{I}\{Z_S\})}, \quad (1)$$

where Z_L is TD impedance, Z_S is source impedance, and Z_S^* represents the complex conjugate of the source impedance [14]. Ignoring the imaginary part for simplification, the equation becomes:

$$\Gamma_{in} = \frac{\mathbf{R}\{Z_L\} - \mathbf{R}\{Z_s\}}{\mathbf{R}\{Z_L\} + \mathbf{R}\{Z_S\}}, \text{ where } \mathbf{R}\{Z_S\} > 0. \quad (2)$$

When TD circuit has negative resistance ($\mathbf{R}\{Z_L\} < 0$), we have

$$|\mathbf{R}\{Z_L\} - \mathbf{R}\{Z_S\}| > |\mathbf{R}\{Z_L\} + \mathbf{R}\{Z_S\}| \Rightarrow |\Gamma_{in}| > 1,$$

which results in the reflected signal being stronger than the original incoming signal, and forms the foundation of TD-based amplification. The phenomenon is called *reflection amplification* and the *signal gain* from reflection power can be computed as $|\Gamma_{in}|^2$.

(2) How to build a TD-AMP? After understanding why TD can be utilized for amplification, however, building a practical TD-based amplifier still introduces several challenges. First, TDs are highly sensitive to impedance variations, while RF systems inherently suffer from lumped-element non-idealities and parasitics at RF frequencies. Even seemingly small parasitic values at the ISM band (*e.g.*, 433 MHz) can significantly affect the TD impedance, inevitably causing a mismatch. In addition, TDs are prone to thermal damage during soldering, creating further implementation difficulties.

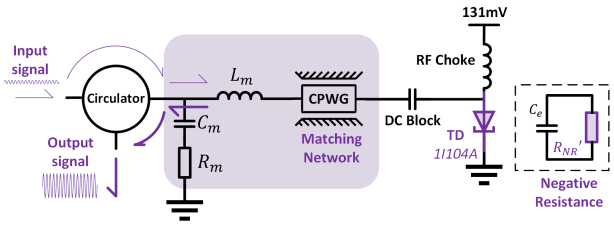

Figure 6: TD-AMP circuit design of Longan.

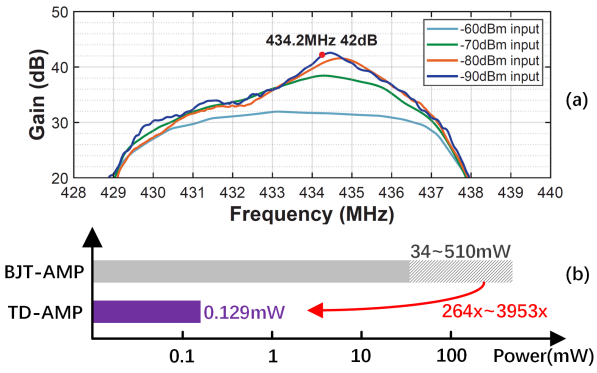

Figure 7: (a) Gain performance of TD-AMP at different input powers (42 dB peak gain @434.2 MHz); (b) Power consumption of TD-AMP versus traditional BJT-AMPs [40, 44].

To address these issues, we introduce a matching network between the signal input and the TD. This network dynamically tunes the reflection amplifier to the target frequency band while adjusting gain. Specifically, we derive a parallel equivalent circuit model, with equivalent capacitance $C_e \approx 2$ pF and equivalent negative resistance $R'_{NR} \approx$ -105 Ω, as shown in Figure 5. After characterizing the TD, we employ a vector network analyzer (VNA) to monitor the input reflection coefficient and fine-tune the component values of the matching network, until an optimal configuration is reached. The overall TD-AMP circuit design is shown in Figure 6. Due to the

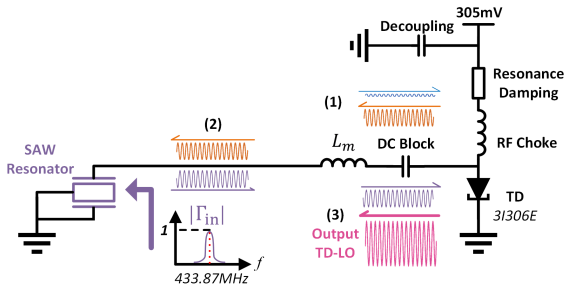

Figure 8: TD-LO circuit design in Longan, inwhich oscillation is generated by repeated reflection and amplification of SAW resonator and TD at a fixed frequency.

sensitivity and variation of tunnel diodes, the overhead of applying this matching operation is necessary for current Longan nodes, but this issue can be remedied (or even eliminated in the future) as the stability of newer TDs (*e.g.*, MBD1057 [14, 16]) improves.

Our matching network consists of L_m, C_m, and R_m, whose values are derived using the above method. To protect the TD from soldering heat, we further design a 0.12λ coplanar waveguide with ground (CPWG) transmission line. With L_m and C_m, this line counteracts the TD's equivalent capacitance C_e, enabling parallel resonance at the target frequency. Finally, as shown in Figure 6, we employ a circulator to separate input and output ports. With 48 dB isolation between the input signal and amplified output, the circulator transforms the reflection amplifier into a standard 2-port RF TD-AMP.

(3) Performance validation. The measurement performance of the TD-AMP is shown in Figure 7. Vector network analyzer measurements across four different input power levels demonstrate a peak gain of 42.27 dB at a center frequency of 434.2 MHz, confirming the excellent amplification capability. In terms of power efficiency, the TD-AMP maintains stable operation while consuming only 0.129 mW. By contrast, conventional BJT-based RF amplifiers [40, 44] typically require between 34 mW and 510 mW to achieve a similar gain, depending on the specific chipset. As a conclusion, Longan's TD-based amplifier achieves a 264× to 3953× power-saving improvement compared with widely adopted BJT-based ones.

3.2 TD-based Local Oscillator (TD-LO)

After RF amplification, the signal is typically down-converted from the RF band to the IF band, which requires a frequency reference generated by a local oscillator (LO). Conventional LO designs rely on phase-locked loops (PLLs), but their power consumption poses a major obstacle for ultra-low-power applications. To overcome this, we propose an ultra-low-power LO design, which requires two key components: amplification and frequency selection.

(1) Amplification. For amplification in LO, we also employ TD as ultra-low-power active devices. When biased in their negative-resistance region, TDs provide sufficient gain for sustained oscillation with significantly lower power than conventional devices (§3.1). To achieve the optimal oscillation performance for the ISM 433 MHz band, we select 3I306E tunnel diodes, which exhibit negative resistance at 0.305 V bias and 0.85 mA current, yielding only 0.26 mW static consumption [18]. Compared to the 1I104A, the 3I306E offers a wider negative resistance region, enabling larger oscillation amplitude and higher LO output power.

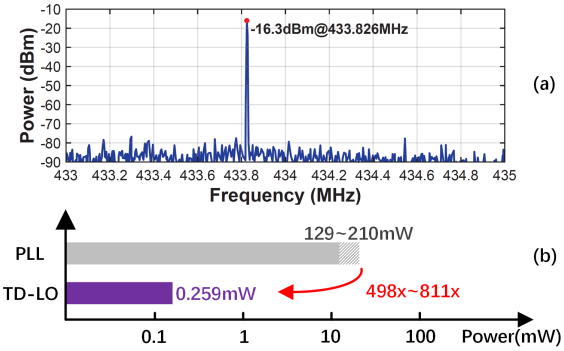

Figure 9: (a) Output of TD-LO achieves stable oscillation at 433.826 MHz with a power of -16.3 dBm; (b) Power consumption of TD-LO versus PLL-based solutions [13, 27].

(2) Frequency selection. A second essential element for oscillation is the frequency-selective feedback network. Conventional frequency selection applies to LC resonators, which suffer from significant temperature drift [5, 63], limited tuning, and low quality factors ($Q < 100$) [6], leading to large phase noise [24]. Inspired by low-frequency TD crystal oscillators [8], we adopt a 433.92 MHz (our local LoRa frequency band) surface acoustic wave (SAW) resonator as the frequency-selective element. SAW resonators provide superior frequency stability [39] and high Q values (>1000) [1], ensuring excellent frequency selectivity and phase-noise performance [37]. Note that Longan is not limited to 433.92 MHz, which can support operation across a wide frequency range from 224.5 MHz to 1.5 GHz. Adapting Longan to other frequency bands only requires replacing the SAW resonator and LC matching network with the one operating at the target frequency.

(3) TD-LO. Combining these two components, TD-LO consists of a TD, a SAW resonator, and other components forming a closed-loop LO system, as depicted in Figure 8. The operation proceeds as follows: (1) the TD functions as a reflection amplifier, boosting system noise at the target frequency and feeding it to the SAW resonator; (2) at resonance, the grounded SAW resonator reflects nearly all signal power back to the TD, since its impedance approaches zero (Eq. 1); and (3) iterative amplification and reflection between the TD and SAW continue until the TD saturates at maximum output power, producing a stable oscillation at the SAW resonant frequency.

(4) Performance validation. As shown in Figure 9, our measurements confirm that the TD-LO achieves a stable 433.826 MHz output with −16.3 dBm power and −101.7 dBc/Hz phase noise (at 11 kHz offset) via a spectrum analyzer, while consuming only 0.259 mW (0.305 V × 0.85 mA). This represents 498× to 811× reduction in power consumption compared to BJT-based PLL solutions [13, 27].

3.3 Down-Conversion Mixer (Mixer1)

With a reliable reference signal generated by the TD-LO, the next step is to down-convert the signal from the RF band to the IF band (for the IF module). One might ask *whether this can be accomplished using a conventional mixer?* Our study suggests that the answer is negative because the TD-LO introduces unique challenges for the mixer design. First, inherited from the TD's bidirectional nature, TD-LO shows inadequate port isolation compared with PLL-based LOs, which will lead to a significant signal leakage between TD-AMP and

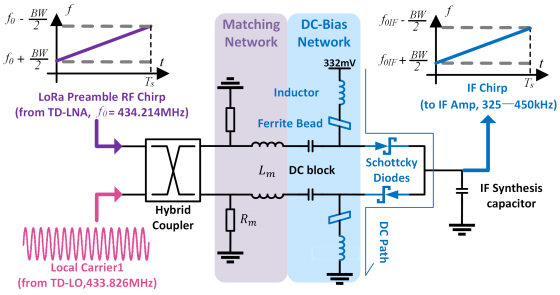

Figure 10: Mixer1 design in Longan that converts RF to IF with reference to local carrier 1. The schottky diodes are biased through inductors and ferrite beads.

TD-LO, severely reducing the effective gain for RF amplification. Second, TD-LO only provides a limited output power of −16.3 dBm, far below the power requirement of a typical mixer driver. These limitations motivate the design of a customized mixer (Mixer1) tailored for Longan, which we introduce below:

(1) Conventional mixer architectures. Conventionally, there are three main mixer technologies commonly used: unbalanced, double-balanced, and single-balanced mixers. Unbalanced mixers are implemented using a single diode. However, they suffer from very poor port isolation, leading to severe LO leakage. Double-balanced mixers provide superior signal isolation (*e.g.*, 30-40 dB) but require ultra-high-power supply from LO drive (7-17 dBm) [35, 36]. Single-balanced mixer achieves 20-30 dB LO-RF isolation with moderate LO drive requirements (*i.e.*, <10 dBm) [9, 28], making it optimal for our TD-based design with limited LO power.

(2) Longan's DC-biasing Mixer1 design. Despite building on single-balanced architecture, the TD-LO's low local carrier output of -16.3 dBm is still insufficient to properly drive the mixing diodes. This limitation causes substantial signal loss (>15 dB) during the RF-to-IF conversion process, degrading the system's reception performance. To address the insufficient TD-LO drive power [9], we propose a *DC-biasing mixing diodes design*, which intentionally sacrifices a small amount of DC power to bias the diodes, thereby reducing low LO power loss and enabling robust mixing performance under low LO power conditions.

However, designing an effective DC bias circuit is also challenging: we need a component that provides a DC voltage bias for the mixing diode while simultaneously preventing the desired signal (RF, LO approximately 433 MHz; IF, 300-600 kHz) from leaking into the DC supply (which also causes significant signal loss). Therefore, this component must block RF and IF signals while providing good DC conduction. Large inductors can suppress IF frequencies, but allow RF signals (RF, LO) to pass through their parasitic capacitance. Small RF inductors block RF but fail to block IF signals. Resistors provide broadband isolation but lack good DC conduction, conflicting with the ultra-low power goal. To overcome this challenge, we innovatively connected a large inductor (high impedance at IF) in series with a ferrite bead (high resistive impedance at RF), which effectively isolates RF and IF signals without the risk of parasitic resonance while providing good DC conduction. In Figure 10, we bias schottky diode pairs [10] to 0.33 V through DC bias circuits, placing them at switching threshold for maximum nonlinearity and lowest RF-IF conversion loss. In this mixer, a hybrid coupler balances the RF signal from TD-AMP and local carrier from TD-LO to the diode pair while providing enough RF-LO isolation. For optimal isolation, symmetric matching networks are inserted between the 50 Ω hybrid coupler outputs and diodes, optimizing diode conditions. At the output, a signal synthesis capacitor undertakes IF signals, directing them to subsequent IF module for processing.

(3) Performance validation. We examine the output of Mixer1 on an oscilloscope. With a -40 dBm RF input at 434.2 MHz and a -16.3 dBm reference signal from the TD-LO, Mixer1 generates an IF signal with a peak-to-peak amplitude of 2.8 mV, corresponding to only a 7.1 dB voltage conversion loss. Spectrum analysis further shows that Mixer1 achieves 25.7 dB isolation (within the typical 20–30 dB range), confirming its effectiveness. The total power consumption of Mixer1 is just 109 μW, primarily from the bias network.

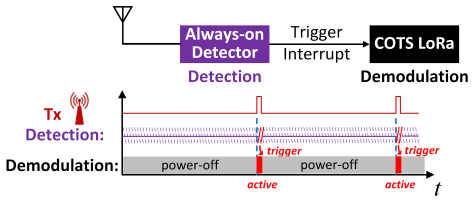

Figure 11: Decouple detection and demodulation in Longan.

4 Packet detector

4.1 Decouple Detection and Demodulation

Although Longan achieves low power consumption in RF amplification and RF-to-IF conversion as described in §3, the subsequent digital-domain IF processing remains a key challenge: In conventional COTS LoRa receivers, digital-domain IF operations, such as analog-to-digital conversion, dechirping, and FFT (Figure 2), are highly effective for packet detection but come with significant power costs (*e.g.*, over 30 mW). This high power demand severely limits their suitability for frequent packet detection and corresponding low-power LPWAN applications.

To address this challenge, inspired by the emerging wake-up receiver paradigm in low power IoT networks [38, 59], we adopt a similar strategy to decouple the complex LoRa chirp-spread-spectrum (CSS) processing into two functional modules – detection and demodulation – to maximize energy efficiency.

• **Detection**. In the detection module, only preamble detection is performed to verify the presence of a valid incoming signal, without decoding any payload data. This simplification drastically reduces power consumption, allowing the detector to even remain always on for continuous monitoring.

• **Demodulation**. Once a preamble is detected, the demodulation module is activated to extract the payload and recover full information. Because the demodulator is only powered during active data demodulation, its wake-up duration is intermittent and much shorter than the detector's continuous operation time. For most of the time, the demodulation module remains in idle mode to minimize power overhead, as illustrated in Figure 11.

Such a decoupled design enables Longan to achieve significantly lower IF & baseband power consumption (e.g., 0.66 mW) even during always-on reception. In contrast, conventional LoRa IF operations require over 30 mW, demonstrating the superior low-power performance of Longan. Thus, the main design challenge lies on the

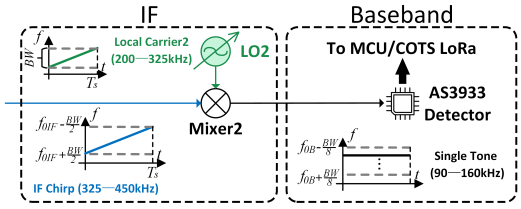

Figure 12: Workflow of the detector design in Longan.

detection side: *How can we design a standalone LoRa baseband detector that delivers high-accuracy packet detection while maintaining low power consumption?* Below, we detail Longan's approach.

4.2 Design Opportunity and Challenge

(1) Existing work. Existing LoRa baseband preamble detection in SOTA designs [57, 64] relies on envelope detectors and face difficulties in maintaining low power consumption while achieving high packet detection sensitivity, making them unsuitable for direct use in Longan. These designs rely on diode-based passive envelope detectors to detect packets after LoRa dechirping. Although this approach is power efficient, passive envelope detectors suffer from limited sensitivity (*e.g.*, < -40 dBm), which significantly degrades packet detection accuracy. Some recent efforts [64] attempt to improve sensitivity by adding dedicated amplifiers and comparators. While these active components enhance detection ability, they must carefully limit the gain of amplifiers to achieve low power consumption, resulting in a slight improvement in sensitivity.

(2) **Opportunity**. Unlike existing methods, Longan uses a low-frequency ASK receiver IC AS3933 [49], for enabling baseband LoRa preamble detection. Originally designed for active RFID tags, the AS3933 is a low-frequency wake-up receiver intended to detect 125 kHz ASK signals. The key advantage of AS3933 lies in its extremely low power consumption, requiring only 5.75 μW, making it suitable for continuous operation. Moreover, due to the advanced integrated design, AS3933 incorporates a high-gain amplifier and dedicated detection circuitry, achieving a sensitivity of -69 dBm, significantly over the -40 dBm sensitivity of existing envelop detectors, allowing it to achieve high packet detection accuracy.

(3) **Challenge**. However, directly using such a low-frequency receiver chip is challenging for LoRa preamble detection, as the dechirped LoRa baseband signal will have a wider frequency range (125 kHz/250 kHz) compared with the limited detection range of the AS3933 between 95 and 150 kHz. That means, if the IF LoRa preamble chirp is not aligned with the reference LO2 used for dechirping, the resulting dechirped baseband signal can drift outside the AS3933's frequency detection range. Consequently, the detection rate performance of Longan will degrade.

To address this challenge, we present our solution for enabling accurate baseband preamble detection on the AS3933 through an analog dechirping synchronization mechanism, detailed below.

4.3 Analog Dechirping Synchronization

In this section, we detail our solution on enabling accurate baseband preamble detection on AS3933, as illustrated in Figure 12.

(1) Phase mismatch during analog dechirping. Analog dechirping requires mixing the incoming IF signal $f_{IF}(t)$ with a reference chirp signal $f_{LO2}(t)$ generated by local oscillator LO2. The $f_{IF}(t)$

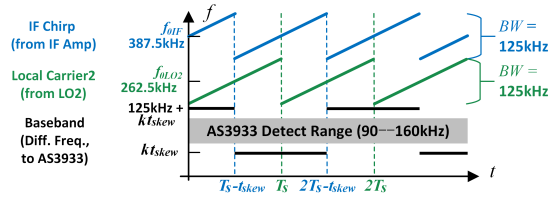

(a) W/o 4-phase-shifting, the offset is random, and the baseband signal is likely outside the detection range of the AS3933 ($t_{skew} = T_s/2$ in this figure).

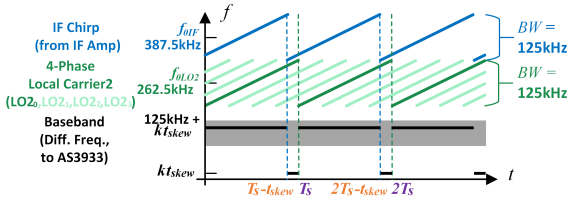

(b) W/ 4-phase-shifting, the offset < $T_s/8$, and the baseband signal is in the detection range of the AS3933 ($t_{skew} = T_s/8$ in this figure).

Figure 13: Comparison of baseband signals w/ and w/o the 4-phase-shifting design for LO2.

and $f_{LO2}(t)$ can be computed as follows:

$$\begin{aligned} f_{IF}(t) &= f_{0IF} - \frac{BW}{2} + k[(t + t_{skew}) \bmod T_s], \\ f_{LO2}(t) &= f_{0LO2} - \frac{BW}{2} + k(t \bmod T_s), \end{aligned} \tag{3}$$

where t_{skew} denotes chirp offset ($t_{skew} = T_s/2$); f_{0IF} and f_{0LO2} are center frequencies of $f_{IF}(t)$ and $f_{LO2}(t)$, respectively, where $f_{0IF} > f_{0LO2} + BW$; BW represents the bandwidth of the LoRa chirp, T_s is the time of a chirp symbol, and the parameter k can be computed through $k = BW/T_s$.

As shown in Figure 13 (a), after dechirping, the frequency differences can be computed through:

$$f_{IF}(t) - f_{LO2}(t) = \begin{cases} f_{0IF} - f_{0LO2} + kt_{skew}, & \text{if } t \in [0, T_s - t_{skew}), \\ f_{0IF} - f_{0LO2} - BW + kt_{skew}, & \text{if } t \in [T_s - t_{skew}, T_s). \end{cases} \tag{4}$$

However, phase misalignment between $f_{IF}(t)$ and $f_{LO2}(t)$ can occur. Without accurate synchronization, uncontrolled chirp offset t_{skew} can shift the baseband frequency by $\pm BW/2$ relative to the center frequency f_{0B}, where $f_{0B} = f_{0IF} - f_{0LO2}$, making the resulting baseband frequency falling outside the detector's 90–160 kHz operating range and significantly reducing detection accuracy. To address this challenge and ensure reliable dechirping, we propose a four-phase shifting synchronization algorithm that generates a properly aligned reference chirp on LO2 for Mixer2, guaranteeing the success of analog dechirping.

(2) Solution: four-phase shifting synchronization algorithm. The key idea is to periodically shift the phase of LO2 to match the random phase of the incoming IF signal.

Specifically, a square wave with period $T_s/4$ is generated by the oscillator (LTC6990) and fed into a modulo-4 ring counter, producing four orthogonal square waves Q_0 to Q_3 with 90° phase differences and a period of T_s. These are input into a multiplexer,

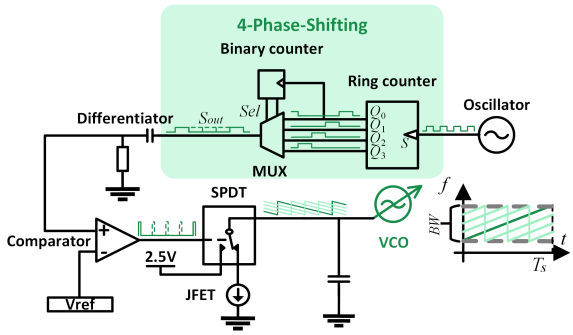

Figure 14: LO2 circuit design in Longan. We use 2 counters and a MUX as the key devices for implementing 4-phase-shifting in LO2. The total power consumption is 0.475 mW.

whose 2-bit select signal, derived from a counter on Q_0, cycles every $4T_s$, shifting the output phase by $T_s/4$ across four distinct phases. A differentiator and low-power comparator (TS881) generate narrow pulses from the rising edge, which control a SPDT switch (TS5A3159). This switch charges or discharges an integrating capacitor (charged to 2.5 V when high, discharged via a constant current source MMBFJ201 JFET when low), producing an inverse sawtooth waveform. The waveform drives a low-frequency VCO (LTC6990), converting voltage into a linearly decreasing frequency to generate the LO2 chirp, as illustrated in Figure 14.

As shown in Figure 13(b), this approach produces four phase-shifted chirps ($LO2_0$ to $LO2_3$), alternating every $4T_s$, which ensures that at least one chirp achieves minimal timing skew (t_{skew}) alignment within 16 IF chirp periods. In the worst case, where $t_{skew} = \pm T_s/8$ occurs when phases are misaligned by half a phase step, it also leads to a maximum frequency offset of ±15.6 kHz (BW = 125 kHz), which remains well within the AS3933 detector's 90–160 kHz range, ensuring reliable preamble detection. Similar result also holds for other bandwidths like BW = 250 kHz.[2] After preamble is detected, Longan uses demodulator to demodulate subsequent symbols to ensure high-quality demodulation performance.

5 putting them together

In addition to the design modules introduced in previous two sections, other components in Longan include:

(1) IF amplification (IFA). Longan requires IF amplification in the 300-600 kHz range while maintaining ultra-low power consumption. Our design employs RF BJTs (2SC3357) operating under extremely low DC bias (1.8V supply, 30-60 μA collector currents) in a 2-stage common-emitter cascade configuration. Despite reduced bias conditions, RF BJTs retain sufficient performance, with each module delivering 8-16 dB gain through emitter AC coupling and inductive frequency compensation. Measurement shows that the IFA achieves 24 dB voltage gain at 450 kHz with 0.162 mW power consumption (1.8 V × 90 μA).

(2) Analog switch mixer (Mixer2). It down-converts and dechirps the amplified IF signal (300–600 kHz) for baseband detection by low-power mixing with LO2. To achieve low-power consumption,

[2]With the four-phase synchronization, the 250 kHz bandwidth exhibits a maximum frequency of ±31.25 kHz, and setting the IF-chirp center frequency to 125 kHz keeps the down-converted signal within the 93.75 to 156.25 kHz range, which falls within the 90 to 160 kHz detection window of the AS3933.

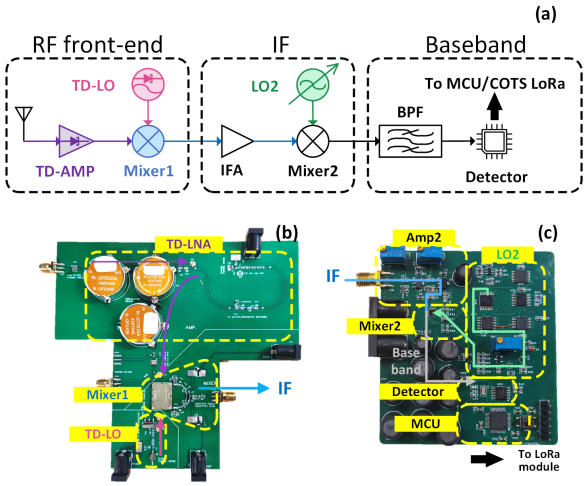

Figure 15: (a) System architecture; (b) RF front-end and (c) IF/baseband designs in the Longan prototype.

we adopt a CMOS analog switch (ADG719), controlled by the LO2 square wave to periodically open and close, multiplying the IF signal to produce sum and difference frequencies. The difference ($|f_{IF} - f_{LO2}|$) yields the desired baseband output. The power consumption is remarkably low at 20 μW (0.02 mW = 1.8 V × 11.1 μA), showing excellent energy efficiency. Oscilloscope verification confirms that the baseband signal is successfully recovered.

(3) Baseband signal detector. We use an AS3933 low-frequency receiver as a novel single-tone detector for the dechirped LoRa preamble [49]. It provides -69 dBm sensitivity at 5.75 μW (2.5 V × 2.3 μA) merely. To prevent false wake-ups at long chirp symbol time T_s and high spreading factors (*e.g.*, SF12), we implement a confirmation logic by detecting multiple consecutive wake-up pulses.

(4) Demodulation operations. The STM32L431CCU6 MCU remains in a 4 μW (2.5 V × 1.6 μA) sleep mode alongside the LoRa module until woken by the AS3933 detector. Upon a confirmed preamble, MCU uses COTS LoRa demodulator to demodulate subsequent symbols to ensure high-quality demodulation performance.

By assembling these components, Longan prototype uses 2 FR4 printed circuit boards (Figure 15): 14.5 cm × 15.7 cm (RF front-end) and 7.0 cm × 7.7 cm (IF/Baseband), connected via SMA interfaces. In RF front-end, 2 SAW filters (433.0–434.7 MHz) suppress out-of-band interference and TDO self-oscillations. For the power supply of Longan, TI TPS7A94 LDO provides sub-1V supplies, and AMS1117-1.8/2.5 provides 1.8 V/2.5 V rails.

(5) Ambient temperature. Our current design and evaluation in §6 primarily consider common ambient temperatures (~20°C). However, the I-V negative resistance voltage range of TDs could change with temperatures (approximately inverse linear relationship with temperature [17, 21]). We plan to explore a thermistor-based bias voltage compensation circuit to adjust the DC bias point of the TDs to adapt to temperature variations in the future.

6 Evaluation

Experiment setup. Across all experiments, the transmitter (Tx) sends over 8,000 packets, each containing 16 bytes of data. Upon detecting a LoRa packet, Longan triggers an external MCU interrupt, waking the MCU and the COTS LoRa transceiver to receive data and

forward it to a gateway. Unless otherwise specified, the bandwidth (BW), carrier frequency (CF), coding rate (CR), and spreading factor (SF) are set to 125 kHz, 434.214 MHz, 4/5, and 8, respectively. The receiver antenna gain is 3 dBi.

Metrics. We use the following metrics for evaluation:

- **Power Consumption:** The receiver's power consumption.
- **Packet Receive Rate (PRR):** The percentage of successfully decoded packets out of all packets.
- **Sensitivity:** The lowest received signal strength indicator (RSSI) value at 90% PRR [52]. The lower the sensitivity, the weaker the signal can be received.
- **Goodput:** The number of packets successfully decoded per minute (pkt/min). The higher the goodput, the more messages the network can successfully transmit per unit time.
- **Latency:** Time between packet generation and reception. The lower the latency, the faster the network responds.

Below, we first evaluate the power consumption and receiver sensitivity of Longan, followed by micro-benchmarks. We then assess the network-wide performance and conclude with a case study under a multi-hop setting.

6.1 Power Consumption

To validate Longan's low-power performance, we measure power consumption using an LPT2020 power monitor, comparing Longan with COTS and state-of-the-art receivers:

• **SX1278 receive [51]:** Classic COTS LoRa transceiver with continuous RF front-end and ADC operation, resulting in high power consumption.

• **SX1268 receive [54]:** Latest COTS transceiver, achieving lower but still significant power consumption.

• **Sisyphus [64]:** Recent low-power LoRa receiver design which eliminates amplifier and local oscillator, requires a reference signal for demodulation.

• **μMote [57]:** Recent LoRa-like chirp signal receiver by introducing two parallel chirps, which also eliminates amplifier and local oscillator for low-power operation.

Both COTS receivers support a LoRa feature, called Channel Activity Detection (**CAD**) [50, 52], which enables brief channel monitoring via narrowband scanning. While MCU limitations prevent continuous monitoring like Longan, we still configure CAD for both modules for a thorough evaluation.

Result. As shown in Figure 16, the power consumption of Longan receiver achieves excellent energy efficiency with the total power consumption of 1.16 mW only. In contrast to conventional receivers, which typically consume tens of mW in amplifier and PLL, the RF front-end of Longan consumes < 500 μW and is not the dominant power consumer. This efficiency stems from innovative TD design and analog-based packet detection, avoiding energy-intensive ADC, FFT, and digital signal processing. Longan achieves 36× to 31× reduction compared to SX1278 in receive mode and CAD mode, respectively. It also achieves 21× and 15× reduction compared to SX1268 in these two modes, respectively.

Under short communication range, the power consumption of Sisyphus and μMote is small, *e.g.*, 449 μW of Sisyphus for about 107 meters and 62.07 μW of μMote for about 400 meters. To further compare with COTS and Longan receivers, we add amplifiers

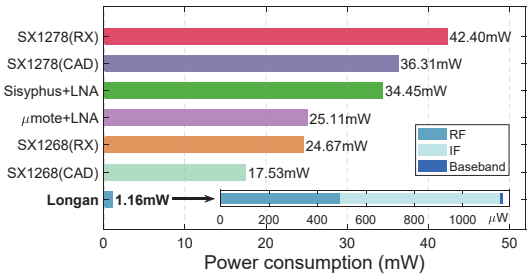

Figure 16: Power consumption comparison between Longan, state-of-the-art low-power receivers, and COTS LoRa receivers over a 1.6 km communication range.

Table 2: Power breakdown of three parts in Longan.

RF			IF			Baseband	
TD-AMP	TD-LO	Mixer1	IFA	LO2	Mixer2	Detector	MCU
128 μW	259 μW	109 μW	162 μW	475 μW	20 μW	6 μW	4 μW

for them to achieve a similar communication range (1.6 km), and Figure 16 reveals their power consumption is comparable to COTS receivers (25–34 mW).

Power breakdown of Longan. Table 2 further reports the power consumption details for each module in Longan. Specifically, IF module accounts for over 56% of the total power consumption, with IFA (162 μW, caused by BJT) and LO2 (475 μW, caused by 2 oscillators) contributing 97% of IF power draw. Future Integrated Circuit (IC) implementation using TSMC's 180 nm CMOS process could reduce IF power from 657 μW to about 25 μW through ultra-low-power operational amplifiers (3–20 μW) [47, 58] and digitally controlled oscillators (~5 μW) [15], which will further halve Longan's overall power consumption.

6.2 Receiving Sensitivity

Receiving sensitivity determines the communication range. Similar to the measurement method adopted in prior study [52], we evaluate the receiving sensitivity by measuring PRRs when varying RSSI levels and SFs. In particular, an SX1268 module is set as the transmitter with an 80 dB cascaded RF attenuator to control signal strength. The transmitting power and communication distance are adjusted to vary RSSI, with signal power calibrated using another SX1268 equipped with Qorvo TQP3M9008 LNA for precise measurement. Since Sisyphus and μMote trade sensitivity for power power (-48 to -40 dBm), we skip the comparison with them.

In Figure 17, we compare Longan with the most advanced COTS SX1268 by varying SF (8,10,12) and BW (125 kHz, 250 kHz). A red horizontal line at 90% PRR serves as the sensitivity threshold, where a smaller RSSI at this intersection indicates better sensitivity. Longan and SX1268 show high similarity across different configurations, with Longan performing slightly less sensitive compared to SX1268. In Figure 17(a) with BW = 125 kHz, both achieve full reception above -123 dBm and lose all packets below -140 dBm. Longan achieves slightly higher RSSI values than the SX1268 at a 90% PRR, dropping by only 3 dB (SF=8) to 13 dB (SF=12) compared to SX1268. Similarly, in Figure 17(b) for BW = 250 kHz, the gap between Longan and SX1268 narrows further to 2–11 dB. Overall, Longan trades certain sensitivity (3–13 dB) for achieving an ultra-low power consumption of 1.16 mW. If a higher sensitivity is

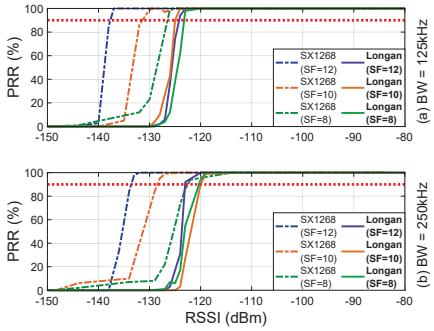

Figure 17: PRR and receiving sensitivity of Longan and COTS SX1268 under various SF settings with (a) BW=125 kHz and (b) BW=250 kHz.

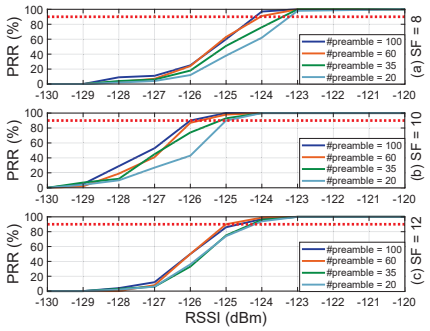

Figure 18: PRR and receiving sensitivity of Longan under different numbers of preamble chirps with (a) SF=8, (b) SF=10, and (c) SF=12.

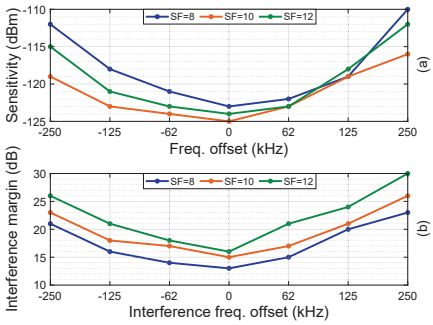

Figure 19: Longan's (a) sensitivity under signals w/ different CFO; (b) interference margin under interference with different frequency offsets.

required, a low-power, active amplifier like LNA can be added to the signal chain. We will empirically investigate this approach in the future.

Note that both receivers tend to have higher sensitivity at higher SF values due to the enhanced signal-to-noise ratio resulting from longer time spreading. However, due to the differences in the AS3933 settings when BW = 125 kHz, Longan's SF = 10 performs slightly better than SF = 12. As discussed in §5, SF = 12 requires more trigger pulses for preamble detection, thus raising the detection threshold to prevent false wakeups. Extending the BW from 125 kHz to 250 kHz results in a 3–6 dB degradation in sensitivity for all systems. This degradation is due to the increased thermal noise during analog dechirping, *i.e.*, the increased thermal noise bandwidth reduces the demodulated signal-to-noise ratio. On the other hand, the degradation in Longan's SF = 10 at BW = 250 kHz stems from the poor gain flatness of low-power IF Amp2, which is an engineering trade-off, not a limitation of the method itself.

6.3 Micro-benchmarks

We then conduct micro-benchmark experiments to evaluate how practical factors affect the performance of Longan.

6.3.1 Effect of # Preamble Chirps. Preamble chirps are the synchronization signal sent at the beginning of each LoRa packet to enable receiver detection. Reducing the number of preamble chirps in a packet generally reduces the probability of triggering receiver to detect the packet. Figure 18 shows the PRR versus RSSI for the Longan receiver (SF=8, 10, 12, BW=125 kHz) by varying the numbers of preamble chirps in a LoRa packet. Fewer preamble chirps (*e.g.*, 100) reduce PRR and sensitivity, attributed to a lower probability of preamble detection. Specifically, when SF = 8, sensitivity ranges from -124 dBm (#preamble=100) to approximately -123 dBm (#preamble=20). Other SF settings also experience a slight performance degradation with fewer preamble chirps. However, the sensitivity fluctuation does not exceed 2 dB, showing that Longan is robust to various settings of the number of LoRa preamble chirps.

6.3.2 Effect of Carrier Frequency Offset. Figure 19(a) shows the sensitivity (*i.e.*, the RSSI value at 90% PRR) versus the carrier frequency offset (CFO) of Longan (BW = 125 kHz; SF = 8,10,12). Within a CFO range of ±62 kHz (BW/2), the sensitivity degradation is limited to 1–2 dB relative to the CFO-free condition, indicating Longan's high

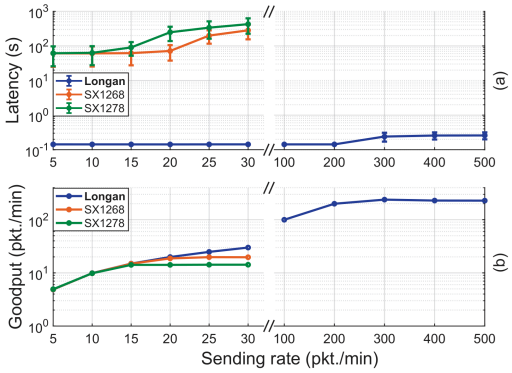

Figure 20: Single link performance of 3 methods under various sending rates in terms of (a) latency and (b) goodput.

robustness against slight CFO induced by temperature or low-cost frequency references. When the CFO is significantly out of band, it is considered as adjacent channel interference rather than a desired signal. Therefore, for signals with large frequency offsets, the Longan receiver becomes less sensitive, and the difference between this sensitivity and optimal sensitivity is defined as adjacent channel selectivity (ACS). For signals with the CFO beyond ±125 kHz (BW), Longan achieves 10—15 dB ACS for SF=8 and SF=12, which can effectively avoid signals to be interfered by adjacent channels. Longan's ACS is lower than that of COTS ones, because as an early attempt at an ultra-low-power LoRa receiver design, Longan prioritizes a trade-off between sensitivity and detection range. One feasible way to improve the ACS is to apply external high-Q SAW filters at the antenna input in highly crowded environments.

6.3.3 Effects of Single-Tone Interference. To understand the anti-interference capability of Longan, we introduce single-tone interference in this experiment and use *interference margin*, defined as the difference between *interference wake-up strength* and *valid LoRa signal sensitivity* to quantify the performance in Figure 19(b). Benefitted from our anti-fake-wakeup design (§5), Longan (at SF=8, 10, and 12) exhibits a 1—4 dB improvement in noise margins across interference frequency offsets. With zero offset, noise margins range from 13—16 dB (SF=8, 12), enabling Longan to selectively detect weak signals while remaining less responsive to single-tone interference. As tone frequency deviates from the center, noise margin increases to 21—30 dB at 250 kHz offset, demonstrating exceptional

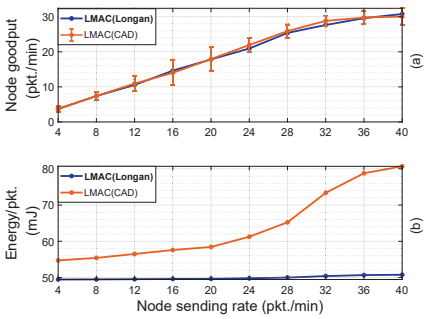

Figure 21: Performance of 2 LMAC protocols under various sending rates in (a) goodput and (b) energy overhead.

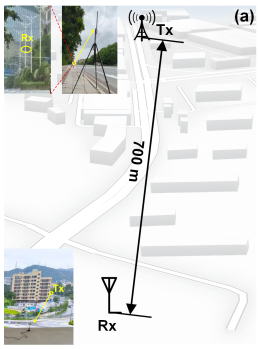

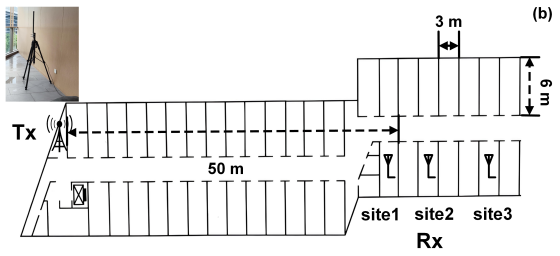

Figure 22: Field map for distance experiments with the SX1268 COTS module and Longan in (a) LOS and (b) NLOS environments.

noise immunity and effective fake wakeup suppression to out-of-band interference.

6.4 Network-Wide Evaluation

In this subsection, we further evaluate the network-layer performance with Longan receiver.

6.4.1 Single link performance. As evaluated in §6.1, the Longan receiver consumes much less power than COTS ones. To harness this advantage, we configure Longan receiver in Class C (always-on), while COTS LoRa receivers are set in Class B with the duty cycles that lead to similar energy consumption to Longan, *e.g.*, the wake-up time is 6 out of 128 seconds for SX1268 and 4 out of 128 seconds for SX1278. In addition, we set up a LoRa transmitter and varies its sending rate from a light-traffic range to a heavy-traffic range (from 5 to 500 pkt/min) to each receiver.

Figure 20(a) shows that the latency of receiving each packet remains small in Longan since it is always awake and can receive packets in time. Due to the relative low duty cycle, two COTS receivers suffer from much higher latencies. When the sending rate is sufficient high (above 100 pkt/min), we find the program of SX1268 and SX1278 receivers halts (no response, likely due to buffer overflow), and we thus skip their latency performance for high sending rates in Figure 20(a). Small latency naturally leaders to higher goodput. As shown in Figure 20(b), the goodput of Longan can scale up to 200 pkt/min as the sending rate increases, but it is limited to 20 and 15 pkt/min for SX1268 and SX1278, respectively.

6.4.2 Power-efficient CSMA. In this subsection, we examine the transmission performance in a LoRa network under the star topology, which contains 9 SX1278 nodes (using CAD) and 1 SX1278 node equipped with Longan receiver. We install the state-of-the-art carrier sense multiple access (CSMA) mechanism LMAC [20] on all 10 nodes for higher network goodput [22, 34, 67, 70]. In this experiment, we vary the average sending rate of each node and monitor the goodput achieved at the gateway.

For clear illustration, we show the average goodput of each type of nodes (using CAD or Longan) in Figure 21(a). We can see that the goodput of two types of nodes is similar, saturated at 30 pkt/min under the sending rate of 40 pkt/min. Using Longan does not affect the network-wide goodput performance, while Figure 21(b) shows that the energy consumption is dramatically different. Leveraging Longan's low-power monitoring, LMAC (Longan) sustains around 50

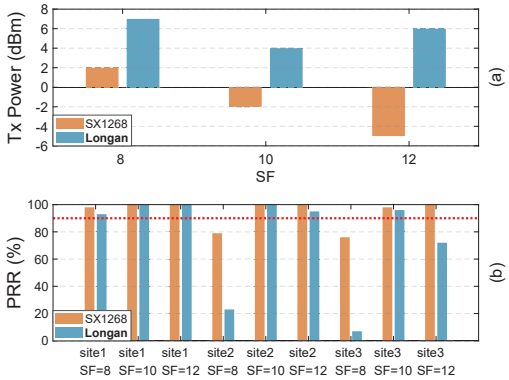

Figure 23: (a) Minimum Tx power for 90% PRR of 2 methods in LOS scenarios; (b) PRR of 2 methods at different locations and SFs under NLOS.

mJ regardless of the sending rate, versus LMAC (CAD)'s 55–80 mJ, reducing per-packet transmission energy by 5.8–37.5%. This shows that Longan is a general design, which is compatible to crucial LoRa techniques (like CSMA) for better network performance.

6.4.3 Long-range and mobile gateway. The advantage of ultra-low power consumption makes Longan a suitable candidate for a mobile gateway or relay node, which may be powered by batteries. In such scenarios, the gateway may receive LoRa packets from line-of-sight (LOS) or non-line-of-sight (NLOS) links. To this end, we conduct experiments as shown in Figure 22(a). We use an SX1268 node as Tx, transmitting packets by varying SF from 8 to 12 at BW = 125 kHz, and Longan receiver as Rx. Tx employs a 6 dBi fiberglass antenna, while receiver (Rx) uses a 3 dBi antenna, well-matched at 434 MHz.

In the LOS scenario, the Tx and Rx are placed 700 m apart outdoors, the furthest LOS distance in our experiment site. Therefore, we adjust the transmit power in 1 dBm increments to determine the threshold for stable reception (PRR > 90%). From Figure 23(a), we can see that under all SF settings, Longan requires a transmit power 4–7 dBm higher than the SX1268 to achieve stable reception, but this is still below the typical LoRa node transmit power of 20–30 dBm. In addition to direct LOS measurements, we also input this link margin at 700 m (and our LoRa configurations) into the official LoRa communication range calculator [56], which translates to a

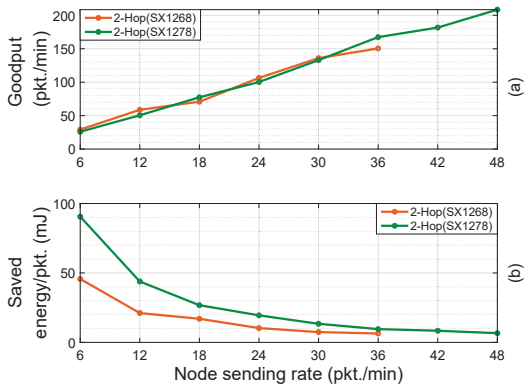

Figure 24: (a) Goodput in Longan-based 2-hop network realized with LoRa modules under various sending rates; (b) Energy consumption savings of Longan-based relay node compared to always-on COTS receivers.

communication range of 1640–1990 m at a standard 20 dBm LoRa transmit power. We will conduct more field tests in our future work.

In the NLOS scenario, Tx is fixed on a balcony at -9 dBm power (SF=8, 10, 12; BW=125 kHz), with SX1268 and Longan placed in various corridor rooms, recording PRR as shown in Figure 22(b). The results show that sites 1, 3, and 5, under complex reflection paths, become the turning points for NLOS reception at SF = 8, 10, and 12, respectively. Their PRR values are shown in Figure 23(b). The performance of Longan is comparable to that of the COTS SX1268 in many scenarios, but Longan may suffer from a sudden drop in PRR when the received signal falls below Longan's sensitivity threshold (-120 dBm). This issue can be remedied by changing the receiver position.

6.5 Case Study: Multi-Hop Network Setting

Finally, we test Longan in a multi-hop network setting, in which a relay node uses Longan with SX1268 and SX1278 as receiver to relay the traffic from 5 two-hop LoRa nodes to the gateway. All the LoRa nodes employ LMAC prior to transmission (SF=8, BW=125 kHz). Figure 24(a) shows that Longan collaborates with COTS LoRa nodes well to support the multi-hop network setting. The goodput, measured at gateway, increases with the node sending rate. The goodput can achieve up to 150–210 pkt/min (the program of SX1268 halts when the sending rate exceeds 36 pkt/min).

In Figure 24(b), we further disable Longan and uses the original COTS receiver in the Class C always-on mode for the relay and examine the energy saving of each rate setting due to Longan. We can see that when the sending rate is not excessively high, the Longan receiver works in the low-power detection mode, which can save a substantial amount of energy per packet. In particular, when the sending rate is 6–24 pkt/min, the energy saving is 10.3–90.6 mJ per packet, which is useful in practical LPWAN networks.

7 Related work

Low-power LoRa receiver. Recent studies have explored low-power LoRa receiver designs [33]. Saiyan [23] employs SAW filters to transform LoRa's frequency-modulated signals into amplitude-modulated ones, enabling envelope detection at 369.4 μW; however, it omits dechirping, effectively operating as a passive FSK receiver without the critical dechirping gain. Similarly, μMote [57] and Sisyphus [64] integrate down-conversion with dechirping via gateway-transmitted dual chirps, achieving zero-power dechirping at the receiver, yielding 400 m range (under 1 W transmit power) at 62.07 μW for μMote and 107 m at 449 μW for Sisyphus. However, by eliminating power-intensive LNAs, these designs cap ranges at hundreds of meters, directly undermining the LoRa's main characteristic of long-range communication. In contrast, Longan leverages TD-based Amp while decoupling detection from demodulation, enabling it to overcome, rather than merely navigate, the power-range tradeoff, delivering kilometer-scale performance at milliwatt levels.

Wake-up receiver. Wake-up receivers provide an energy-efficient paradigm for on-demand IoT activation, keeping devices in deep sleep until triggered. Notable examples include ARISTOTLE [38] for battery-less sensor networks, WakeLoc [11] for precise ultra-low-power localization, and WakeMod [48] with -72.6 dBm sensitivity at 6.9 μW. However, most designs target simple modulations like OOK and are confined to sub-100 m ranges [31, 59], while advanced systems like Zippy [60] and UWB-based wake-ups [43] achieve beyond -70 dBm sensitivity but still fall short of 1 km. Longan distinguishes itself as the first wake-up receiver optimized for complex LoRa chirp-spread-spectrum signals, operating at 1.16 mW and achieving a kilometer-scale range.

TD applications. TD-based backscatter communication designs have achieved significant range improvements with μW-level power consumption [2, 3, 14, 61–63]. Pioneering works like TunnelScatter [62] and Tunnel Emitter [61] introduce tunnel diodes for ultra-low-power backscatter tags, while Judo [63] tackle energy asymmetry. The harmonic tunneling tag [3] explores dual-band operations, and GPSMirror [14] amplify GPS signals via using TD backscatter. While previous works [61, 62] also use TDs, they primarily employ the single-port nature of TDs for backscattering communication, where input and output signals cannot be isolated for active processing. In contrast, Longan leverages the TDs to further build high-isolation, two-port active LNA of ultra-low-power consumption for long-range active communication. This requires input/output signal separation and active signal processing.

8 Conclusion

This paper represents Longan, an innovative LoRa receiver design, overcoming the longstanding power-range tradeoff boundary by enabling km-scale communication with 36× power reduction over commercial counterparts. Through novel tunnel diode-based RF amplification and decoupled analog packet detection, it achieves high sensitivity and efficiency without compromising LoRa compatibility. We develop a Longan prototype and conduct extensive experiments to evaluate its performance and potential in LPWANs, unlocking energy-efficient MAC protocols and multi-hop networking.

Acknowledgments

We thank all the reviewers. This work is supported by the General Research Fund (GRF) grant from Research Grants Council of Hong Kong (CityU 11202623). The corresponding author is Zhenjiang Li.

References

[1] Yujie Ai, Hongrui Lv, Yinglong Huang, Jiaheng He, Ye Wang, Jiwen Wu, and Yun Zhang. 2023. AlN/Sapphire-Based SAW Resonators With Q Over 10000 for Temperature Sensors. *IEEE Sensors Journal* (2023).

[2] Francesco Amato and Gregory D. Durgin. 2018. Tunnel Diodes for Backscattering Communications. In *Proc. of IEEE URSI AT-RASC*.

[3] Francesco Amato and Simon Hemour. 2019. The Harmonic Tunneling Tag: a Dual-Band Approach to Backscattering Communications. In *Proc. of IEEE RFID-TA*.

[4] Aloÿs Augustin, Jiazi Yi, Thomas Clausen, and William Mark Townsley. 2016. A Study of LoRa: Long Range & Low Power Networks for the Internet of Things. *Sensors* (2016).

[5] Mahdi Bagheri, Rahim Bagheri, James F. Buckwalter, and Lawrence E. Larson. 2018. Temperature Sensitivity of Non-Degenerate Modes in CMOS LC Quadrature Oscillators. *IEEE Transactions on Circuits and Systems II: Express Briefs* (2018).

[6] Dirk Bormann, Tobias D. Werth, Niklas Zimmermann, Ralf Wunderlich, and Stefan Heinen. 2008. A comparison of bandwidth setting concepts for Q-enhanced LC-tanks in deep-sub micron CMOS processes. In *Proc. of IEEE ICECS*.

[7] Jiani Cao, Jiesong Chen, Chengdong Lin, Yang Liu, Kun Wang, and Zhenjiang Li. 2024. Practical gaze tracking on any surface with your phone. *IEEE Transactions on Mobile Computing* (2024).

[8] General Electric Company. 1969. *GE Transistor Manual.* https://books.google.com.hk/books?id=rHS2zwEACAAJ

[9] Hewlett Packard Company. 1986. The Schottky Diode Mixer–Application Note 995. http://www.hp.woodshot.com/hprfhelp/4_downld/lit/diodelit/an995.pdf

[10] Skyworks Company. 2024. Surface-Mount Mixer and Detector Schottky Diodes. https://www.mouser.com/datasheet/2/472/Surface_Mount_Schottky_Diodes_200041AH-3364421.pdf

[11] Silvano Cortesi, Christian Vogt, and Michele Magno. 2025. WakeLoc: An Ultra-Low Power, Accurate and Scalable On-Demand RTLS using Wake-Up Radios. In *arXiv:2504.20545*.

[12] Massimiliano De Luca, Pierpaolo Loreti, Lorenzo Bracciale, Giuliano Colosimo, Gabriele Gentile, Francesca Mastrangeli, Glenn P. Gerber, Jane Haakonsson, George Waters, Valerio Allegra, Rosamaria Capuano, Corrado Di Natale, and Alexandro Catini. 2025. Design of a LoRa-Based Multisensor Device for the Internet of Animals. *IEEE Internet of Things Journal* (2025).

[13] Analog Devices. 2012. Wideband Synthesizer with Integrated VCO. https://www.analog.com/media/en/technical-documentation/data-sheets/adf4351.pdf

[14] Huixin Dong, Yirong Xie, Xianan Zhang, Wei Wang, Xinyu Zhang, and Jianhua He. 2023. GPSMirror: Expanding Accurate GPS Positioning to Shadowed and Indoor Regions with Backscatter. In *Proc. of ACM MobiCom*.

[15] Luis Felipe Machado Dutra, Alessandro G. Girardi, and Lucas Compassi-Severo. 2022. A 0.3 to 5-MHz Low-Voltage Digitally-Controlled Oscillator for Energy Harvesting Applications. In *Proc. of SenSysSBC/SBMicro/IEEE/ACM SBCCI*.

[16] EclipseMDI. 2012. MBD1057 Datasheet. https://www.eclipsemdi.com/wp-content/uploads/2021/07/mbd1057-C18-x.pdf

[17] W. Abd El-Basit, Z.I.M. Awad, S.A. Kamh, and F.A.S. Soliman. 2020. Temperature dependence of backward tunnel diode oscillator circuit. *Microelectronics Journal* (2020).

[18] Electronics and Communications Company. 2017. 3I306E - technical characteristics, parameters, description, datasheet. https://eandc.ru/pdf/diod/3i306.pdf

[19] H.T. Friis. 1944. Noise Figures of Radio Receivers. *Proceedings of the IRE* (1944).

[20] Amalinda Gamage, Jansen Christian Liando, Chaojie Gu, Rui Tan, and Mo Li. 2020. LMAC: efficient carrier-sense multiple access for LoRa. In *Proc. of ACM MobiCom*.

[21] Sylvester P. Gentile. 1962. *Basic theory and applications of tunnel diodes.* D.Van Nostrand Company Inc.

[22] Branden Ghena, Joshua Adkins, Longfei Shangguan, Kyle Jamieson, Philip Levis, and Prabal Dutta. 2019. Challenge: Unlicensed LPWANs Are Not Yet the Path to Ubiquitous Connectivity. In *Proc. of ACM MobiCom*.

[23] Xiuzhen Guo, Longfei Shangguan, Yuan He, Nan Jing, Jiacheng Zhang, Haotian Jiang, and Yunhao Liu. 2022. Saiyan: Design and Implementation of a Low-power Demodulator for LoRa Backscatter Systems. In *Proc. of USENIX NSDI*.

[24] E. Hegazi, H. Sjoland, and A.A. Abidi. 2001. A filtering technique to lower LC oscillator phase noise. *IEEE Journal of Solid-State Circuits* (2001).

[25] Quy Lam Hoang, Woo-Sung Jung, Taehyun Yoon, Daeseung Yoo, and Hoon Oh. 2020. A Real-Time LoRa Protocol for Industrial Monitoring and Control Systems. *IEEE Access* (2020).

[26] Ningning Hou, Xianjin Xia, and Yuanqing Zheng. 2023. Don't Miss Weak Packets: Boosting LoRa Reception with Antenna Diversities. *ACM Transactions on Sensor Networks* (2023).

[27] Texas Instruments. 2016. LMX2571 Low-Power, High-Performance PLLatinum™ RF Synthesizer with FSK Modulation. https://www.ti.com/lit/ds/symlink/lmx2571.pdf

[28] Denis. Jaisson. 1992. A Single-Balanced Mixer with a Coplanar Balun. *Microwave Journal* (1992).

[29] Shenyao Jiang, Hao Zhou, Wangqiu Zhou, Xinyu Wang, Zhenjiang Li, and Yusheng Ji. 2025. FREAUTH+: A Robust Frequency Feature-Based Device Authentication Mechanism for Magnetic Wireless Power Transfer System. *IEEE Transactions on Mobile Computing* (2025).

[30] A K Jonscher. 1961. The physics of the tunnel diode. *British Journal of Applied Physics* (1961).

[31] Giannis Kazdaridis, Nikos Sidiropoulos, Ioannis Zografopoulos, and Thanasis Korakis. 2021. A Novel Architecture for Semi-Active Wake-Up Radios Attaining Sensitivity Beyond -70 dBm: Demo Abstract. In *Proc. of ACM/IEEE IPSN Demo*.

[32] Mingzhe Li, Zhen Xiao, Cui Zhao, and Zhenjiang Li. 2025. Using Weak Light Sources to Power Sensor Nodes for Sustainable IoT. In *Proc. of IEEE INFOCOM*.

[33] Songfan Li, Hui Zheng, Chong Zhang, Yihang Song, Shen Yang, Minghua Chen, Li Lu, and Mo Li. 2022. Passive DSSS: Empowering the Downlink Communication for Backscatter Systems. In *Proc. of USENIX NSDI*.

[34] Jansen C. Liando, Amalinda Gamage, Agustinus W. Tengourtius, and Mo Li. 2019. Known and Unknown Facts of LoRa: Experiences from a Large-scale Measurement Study. *ACM Transactions on Sensor Networks* (2019).

[35] Mini-Circuits. 2017. Surface Mount Frequency Mixer ADE-1+. https://www.minicircuits.com/pdfs/ADE-1+.pdf

[36] Mini-Circuits. 2017. Surface Mount Frequency Mixer RMS-1MH+. https://www.minicircuits.com/pdfs/RMS-1MH+.pdf

[37] G.K. Montress, T.E. Parker, M.J. Loboda, and J.A. Greer. 1988. Extremely low-phase-noise SAW resonators and oscillators: design and performance. *IEEE Transactions on Ultrasonics, Ferroelectrics, and Frequency Control* (1988).

[38] Sayedsepehr Mosavat, Matteo Zella, Marcus Handte, Alexander Julian Golkowski, and Pedro José Marrón. 2023. Experience: ARISTOTLE: wAke-up ReceIver-based, STar tOpology baTteryLEss sensor network. In *Proc. of ACM/IEEE IPSN*.

[39] Natalya F. Naumenko. 2021. Temperature Behavior of SAW Resonators Based on $LiNbO_3$/Quartz and $LiTaO_3$/Quartz Substrates. *IEEE Transactions on Ultrasonics, Ferroelectrics, and Frequency Control* (2021).

[40] NXP. 2010. MC13852 General Purpose Low Noise Amplifier with Bypass Switch. https://www.nxp.com.cn/docs/en/data-sheet/MC13852.pdf

[41] Sarah Ouerghemmi, Ahmed Fakhfakh, and Faouzi Derbel. 2025. A Low-Power 868 MHz BJT-Based LNA with Microstrip Matching for Wake-Up Receivers in IoT Applications. *Electronics* (2025).

[42] Sarah Ouerghemmi, Ilef Ketata, Salwa Sahnoun, and Faouzi Derbel. 2021. Performances Analysis of Low Noise Amplifier Based on BJT for Power Aware Wake-Up Receiver Nodes. In *Proc. of IEEE SSD*.

[43] Tommaso Polonelli, Federico Villani, and Michele Magno. 2021. Ultra-Low Power Wake-Up Receiver for Location Aware Objects Operating with UWB. In *Proc. of IEEE WiMob*.

[44] Qorvo. 2024. TQP3M9008 High Linearity LNA Gain Block. https://www.qorvo.com/products/d/da005504

[45] Usman Raza, Parag Kulkarni, and Mahesh Sooriyabandara. 2017. Low Power Wide Area Networks: An Overview. *IEEE Communications Surveys & Tutorials* (2017).

[46] Behzad Razavi. 2011. *RF Microelectronics (2nd Edition).*

[47] Mario Renteria-Pinon, Jaime Ramirez-Angulo, and Alejandro Diaz-Sanchez. 2020. Simple Scheme for the Implementation of Low Voltage Fully Differential Amplifiers without Output Common-Mode Feedback Network. *Journal of Low Power Electronics and Applications* (2020).

[48] Lukas Schulthess, Silvano Cortesi, and Michele Magno. 2025. WakeMod: A 6.9uW Wake-Up Radio Module with -72.6dBm Sensitivity for On-Demand IoT. In *arXiv:2505.21529*.

[49] Sciosense. 2015. AS3933 3D Low Frequency Wakeup Receiver Datasheet. https://www.sciosense.com/wp-content/uploads/2023/12/AS3933-Datasheet.pdf

[50] Semtech. 2013. AN1200.17: Low Energy Consumption Design. https://semtech.my.salesforce.com/sfc/p/E0000000JelG/a/2R0000001OK4/K1xBJSCPflEbqU03CfABAjL29tRKA9KsdAdTIsWBA8s

[51] Semtech. 2020. LoRa Connect Transceiver, SX1278, 137MHz to 525MHz. https://www.semtech.com/products/wireless-rf/lora-connect/sx1278

[52] Semtech. 2023. AN1200.48: LoRa Channel Activity Detection (CAD) with SX126x. https://semtech.my.salesforce.com/sfc/p/#E0000000JelG/a/3n000000qSr4/Xiw4e8ILqgomeM1NnGagqaWbhhLtey7CDNtaHA5JZMs

[53] Semtech. 2024. LoRaWAN® Device Classes. https://www.semtech.com/uploads/technology/LoRa/lorawan-device-classes.pdf

[54] Semtech. 2025. LoRa Connect Transceiver, SX1268, +22dBm, China Frequency Bands. https://www.semtech.com/products/wireless-rf/lora-connect/sx1268

[55] Semtech. 2025. LoRa Technology Overview. https://www.semtech.com/lora

[56] Semtech. 2025. LoRa® Calculator | Semtech. https://www.semtech.com/design-support/lora-calculator

[57] Yihang Song, Li Lu, Jiliang Wang, Chong Zhang, Hui Zheng, Shen Yang, Jinsong Han, and Jian Li. 2023. μMote: enabling passive chirp de-spreading and μW-level Long-Range downlink for backscatter devices. In *Proc. of USENIX NSDI*.

[58] Shikha Soni, Vandana Niranjan, and Ashwni Kumar. 2022. Design of high gain and high bandwidth operational transconductance amplifier (OTA). *International Journal of Electronics* (2022).

[59] Dora Spenza, Michele Magno, Stefano Basagni, Luca Benini, Mario Paoli, and Chiara Petrioli. 2015. Beyond duty cycling: Wake-up radio with selective awakenings for long-lived wireless sensing systems. In *Proc. of IEEE INFOCOM*.
[60] Felix Sutton, Bernhard Buchli, Jan Beutel, and Lothar Thiele. 2015. Zippy: On-Demand Network Flooding. In *Proc. of ACM SenSys*.
[61] Ambuj Varshney and Lorenzo Corneo. 2020. Tunnel emitter: tunnel diode based low-power carrier emitters for backscatter tags. In *Proc. of ACM MobiCom*.
[62] Ambuj Varshney, Andreas Soleiman, and Thiemo Voigt. 2019. TunnelScatter: Low Power Communication for Sensor Tags using Tunnel Diodes. In *Proc. of ACM MobiCom*.
[63] Ambuj Varshney, Wenqing Yan, and Prabal Dutta. 2022. Judo: addressing the energy asymmetry of wireless embedded systems through tunnel diode based wireless transmitters. In *Proc. of ACM MobiSys*.
[64] Han Wang, Yihang Song, Qianhe Meng, Zetao Gao, Chong Zhang, and Li Lu. 2024. Sisyphus: Redefining Low Power for LoRa Receiver. In *Proc. of ACM MobiCom*.
[65] Kun Wang, Jiani Cao, Zimu Zhou, and Zhenjiang Li. 2024. Swapnet: Efficient swapping for dnn inference on edge ai devices beyond the memory budget. *IEEE Transactions on Mobile Computing* (2024).
[66] Xianjin Xia, Ningning Hou, Yuanqing Zheng, and Tao Gu. 2023. PCube: Scaling LoRa Concurrent Transmissions with Reception Diversities. *ACM Transactions on Sensor Networks* (2023).
[67] Xianjin Xia, Yuanqing Zheng, and Tao Gu. 2019. FTrack: parallel decoding for LoRa transmissions. In *Proc. of ACM SenSys*.
[68] Huatao Xu, Liying Han, Qirui Yang, Mo Li, and Mani Srivastava. 2024. Penetrative AI: Making LLMs Comprehend the Physical World. In *Proc. of ACM HotMobile*.
[69] Huanqi Yang, Hongbo Liu, Chengwen Luo, Yuezhong Wu, Wei Li, Albert Y. Zomaya, Linqi Song, and Weitao Xu. 2022. Vehicle-Key: A Secret Key Establishment Scheme for LoRa-enabled IoV Communications. In *Proc. of IEEE ICDCS*.
[70] Cui Zhao, Zhenjiang Li, Han Ding, Wei Xi, Ting Liu, Ruowei Gui, and Jinsong Han. 2022. A Fingertip Profiled RF Identifier. *IEEE Transactions on Mobile Computing* (2022).
[71] Renjie Zhao, Kejia Wang, Kai Zheng, Xinyu Zhang, and Vincent Leung. 2023. SlimWiFi: Ultra-Low-Power IoT Radio Architecture Enabled by Asymmetric Communication. In *Proc. of USENIX NSDI*.